High precision wavelength measurements of QED−sensitive forbidden transitions in highly charged argon ions

I. Dragani?[1?], J. R. Crespo López−Urrutia[1], R. DuBois[2], S.Fritzsche[3], V. M. Shabaev[1,4], R. Soria Orts1,I. I. Tupitsyn[1,4], Y. Zou[5] and J. Ullrich[1]

[1]Max−Planck Institut für Kernphysik, Saupfercheckweg 1, D−69117 Heidelberg, Germany
[2]University of Missouri−Rolla, Physics Building, Rolla, MO 65409−0640, USA
[3]Department of Physics, University of Kassel, Heinrich−Plett−St. 40, D−34132 Kassel, Germany
[4]St. Petersburg State University, Oulianovskaya 1, Petrodvorets, St. Petersburg 198504, Russia
[5]Applied Ion Beam Physics Lab, Fudan University, Shanghai 200433, P. R. China

We present the results of an experimental study of magnetic dipole (M1) transitions in highly charged argon ions (Ar X, Ar XI, Ar XIV, Ar XV) in the visible spectral range. Their wavelengths were determined with for highly charged ions unprecedented accuracy up to the sub−ppm level using an electron beam ion trap, and were compared with theoretical calculations. The QED contributions, calculated in this work, are found to be four orders of magnitude larger than the experimental error for the Be−like and B−like transitions, and are absolutely indispensable to bring theory and experiment to a good agreement. This method shows a great potential for the study of QED effects in relativistic few−electron systems.

PACS number(s): 31.15.Ar, 31.30.Jv, 32.10.Fn, 32.30.Jc, 32.70.Jz

Forbidden transitions, which play a vital role in the temperature and density diagnostics of both laboratory [1] and astrophysical plasmas [2], were first identified in the solar corona by B. Edlén [3]. In more recent years, the major advances in using spectral lines and, in particular, forbidden lines in the analysis of astrophysical plasmas have been successfully transferred to the diagnostics of fusion plasmas, e.g. in tokamak devices. Argon, the element under study in this work, is often chosen for injection into tokamaks for plasma diagnostics. Apart from these applications, precise

---

[?] Present address: The Institute of Nuclear Sciences "Vin?a", Laboratory of Physics (010), P.O. Box 522, 11001 Belgrade, Yugoslavia, e−mail address: draganic@rt270.vin.bg.ac.yu

wavelength measurements of magnetic dipole transitions (M1) in few−electron highly charged ions can provide sensitive tests for *ab initio* and semi−empirical theoretical atomic structure calculations [4−10]. At present, no calculations can reproduce the wavelengths at the level of accuracy obtained in this work.

Furthermore, theoretical calculations show QED contributions to the measured transitions energies as large as 0.3% of the total. The size of these effects, combined with the fact that four− and five−electron systems are becoming tractable for *ab initio* QED calculations (see, e.g. Ref. [11]), as well as comparatively amenable to many−body atomic structure calculations, places these measurements among the most sensitive to QED contributions in highly charged ions. Our experimental data can only be correctly reproduced by including QED radiative corrections and, in fact, the best agreement has been obtained in this way.

In recent years, the full QED treatment of bound electrons has advanced stepwise from the hydrogenic systems to the Li−like sequence. The analytical and numerical methods, developed during this process, can now be applied to the next levels of structural complexity. Nonetheless, the necessary calculations still present a formidable challenge. Here we demonstrate an experimental test with the highest sensitivity and potentially very small theoretical uncertainties in the electron−electron correlation field, which makes further refinement both worthwhile and rewarding.

We measured the wavelengths of the M1 transitions of Ar X $2s^2\ 2p^5\ {}^2P_{3/2}\ -\ {}^2P_{1/2}$, Ar XI $2s^2\ 2p^4\ {}^3P_2\ -\ {}^3P_1$, Ar XIV $2s^2\ 2p\ {}^2P_{1/2}\ -\ {}^2P_{3/2}$, and Ar XV $2s\ 2p\ {}^3P_1\ -\ {}^3P_2$. These measurements were done exploiting the very favourable conditions offered by an electron beam ion trap (EBIT) for high−resolution spectroscopy studies on highly charged ions. A good general reference to EBITs and their applications to atomic physics can be found in [12]. The argon lines have been previously studied by Edlén in 1982 [13] and 1983 [10,14], and, also with an EBIT, by Bieber *et al.* [15].

In the present work, we developed a new approach for precise wavelength determinations, obtaining accuracies up to sub–ppm level. Error sources from statistics, calibration line uncertainties, cut–off of high order of calibration functions, collision and Doppler broadening, Zeeman and Stark effects, as well as detector imperfections and temperature drifts during the measurements were carefully taken into account.

The experiment was performed on the FreEBIT device (now H–EBIT at MPI–K Heidelberg) at the University of Freiburg. The energy of the electron beam used for ionization was set to E_{beam}=1010 eV, with moderate beam currents of 45–50 mA. Argon was introduced into the trap region through a three–stage differentially pumped gas injection system. All working and adjustment parameters of EBIT were kept stable during the measurements.

Photons in the visible range were transmitted from the trap through 2 pairs of quartz lenses with the help of three mirrors to the entrance slit of a JY TRIAX 550 spectrograph equipped with a cryogenic CCD camera (2000x800 pixels on a 30x12 mm^2 chip) with a high quantum efficiency (40% −90%). Detector noise levels are extremely low. The entrance slit of the spectrograph was set to 50 ?m as a compromise between line intensity and resolution. The individual exposure time was chosen to obtain at least about 1500 counts for weak lines and up to 100 000 counts for strong lines (from a few minutes to one hour). The pixels located on the central 2 mm stripe on the detector were vertically binned (200 pixels) *i. e.*, in the non–dispersive direction. Coma and other non–paraxial aberrations, which can cause deviations from the ideal line profile were thus extremely reduced. A typical result for a coronal line is shown in Fig.1. Lines from highly charged ions are typically three times broader (i.e., about 0.1 nm) than calibration lines (around 0.3 nm) due to the Doppler broadening caused by the thermal motion of the trapped ions. Calibration

3

spectra containing several well known lines were recorded before and after each exposure. A diffuse reflector (illuminated with appropriate spectral lamps) was placed at the position of an intermediate real image of the trapped ions. With this choice, the positioning of the reflector became uncritical, as tests showed. For each new exposure, the grating was slightly rotated. A new exposure, with its corresponding calibrations, was then recorded. The entire process was repeated as many as thirty times for each forbidden line. In this way, the statistical limitations posed by too few pixels illuminated across the width of a spectral line were overcome. Non−linear detector response effects for the individual pixels or other flaws became negligible as the sampled line profile contains several hundred individual data points times 200 pixels. One can imagine each pixel as an individual "exit slit", and the procedure described here as the recording of the spectrum with many single detectors by slowly rotating the grating.

Each spectrum was evaluated by fitting individual Gaussian functions to each of the calibration lines to determine their positions, plotting them versus their recommended wavelengths, and using a least−square−algorithm to obtain a second−degree polynomial for the dispersion function. Since the deviation from linear dispersion for this type of spectrograph is small, a quadratic function already provides a very good approximation to the real dispersion. Figure 2 shows the deviation from the dispersion function fitted by linear, second, and third order of polynomial functions. As it can be seen, the difference between the third and the second order polynomial dispersion functions is not obvious and almost purely statistical. The effect of deviations of the line profile from the ideal Gaussian shape was checked by varying the intervals around the line center for the fitting procedure. This was done in order to take into account background, scattered light, Zeeman effect, coma aberration and so on, which could affect the line shape. Within reasonable fitting

intervals, average centroid shifts of about 0.004 pixel, or $3.5 \cdot 10^{-5}$ nm were observed, well below the statistical uncertainty. In this work, we can also neglect shifts of the central wavelength caused by Stark effect, below 10^{-7} nm, by collisions, 10^{-12} nm, and by Paschen−Back effect, 10^{-6} nm, which were all estimated from standard formulae. Other possible sources of systematic deviations like temperature drift etc. are ruled out by our repeated calibration procedure. The main error sources together with their contributions to the final uncertainties are listed in Table 1. All random uncertainties (line centroid errors, standard deviations of wavelength calibration function) have been calculated as a "root sum of squares", whereas systematic calibration errors and uncertainties from calibration lines have been added linearly. Natural argon was used, which contains ^{40}Ar almost exclusively (99.6%).

As can be seen in Table 2, in comparison with other experiments, our experimental results for Ar^{9+} represent almost two orders of magnitude improvement in comparison with the previous most accurate data [19]. For Ar^{10+}, Ar^{13+}, and Ar^{14+}, Bieber *et al.* have reported very accurate values [15]. Still, in our work the respective accuracies have been improved by factors of five to thirty. At this level we have found discrepancies between our results and theirs for the lines of Ar^{13+} and Ar^{14+}, 0.0059 nm for Ar^{13+} and 0.015 nm for Ar^{14+} respectively. Therefore, we performed a second, completely independent measurement for Ar^{13+} after the Fre−EBIT had been moved to Heidelberg, and using a different set of calibration lines. The two results from our independent measurements agree with each other within error bars, giving us confidence in our quoted error estimates.

Our first theoretical approach has been the use of a series of multi−configuration Dirac−Fock (MCDF) computations. Effects from the core−polarization and core−core correlations were considered and compared with the zero order

approximation. Both the experimental and theoretical results from this and other works are listed in Table 2. The theoretical results are at least two or three orders of magnitudes lower in accuracy. It is obvious that semi−empirical calculations are in better agreement with our results. The wavelengths predicted by Kaufman et al [17], are 0.012 nm away from our experimental results for Ar^{9+} . The predictions by Edlén for Ar^{10+}, Ar^{13+}, and Ar^{14+}, are 0.09 nm, 0.06 nm and 0.02 nm, respectively, different from our experimental wavelengths. The agreement for *ab initio* MCDF calculations is less satisfying, usually several tens of nm away from our experimental results. The closest wavelength, from MCDF calculation by Das *et al.* [5], deviates 0.06 nm from our result of Ar^{13+}. From our own MCDF calculations one can see that taking into account the core−valence and core−core correlations does indeed improve the theoretical value, even though the final results are still not satisfactory.

A substantially enhanced agreement is reached when QED contributions are taken into account. In this work, the large−scale configuration−interaction (CI) Dirack−Fock (DF) method was used to calculate the energies of the forbidden transitions. The many−electron wave function with quantum numbers γ J was expanded in terms of a large number of the configuration state functions (CSFs) with the same J. For the occupied shells the orbital basis was generated by the multiconfiguration DF method. The other one−electron states were obtained by solving the Dirack−Fock−Sturm equations. The restricted active space method with single, double, and triple excitations was used to generate the set of CSFs. The total number of CSFs was taken to be about 470 000 for Ar^{+13} and 150 000 for Ar^{+14} .The QED contributions were evaluated by using the one−electron Lamb shift data taken from [25] with an effective nuclear charge number Z_{eff}. For a given one−electron state, Z_{eff} was chosen to reproduce the related DF electron charged density at the Compton wavelength distance from the nucleus. In the case of Ar^{+14}, our value for the

QED contribution agrees well with Sapirstein's result presented in [9]. The results of the calculations are displayed in Table 3. They show excellent agreement with the experimental results. Their estimated theoretical uncertainties are lower than those of other *ab initio* calculations. In future, more elaborate evaluations of the electronic structure will allow to extract QED information from the experimental results.

In conclusion, highly precise experimental wavelengths of ground configuration M1 transitions of highly charged Ar ions were obtained in this work. The accuracy reached up to the 0.23 ppm level, 30 times higher than the previous record for this kind of transitions. To the best of our knowledge, these are also the most precise wavelength measurements for highly charged ions reported until now in any spectral range. Discrepancies between *ab initio* calculations and experimental results are revealed, thus, calling on refined higher accurate modern relativistic atomic structure calculations. Inclusion of QED effects seems mandatory for a satisfactory agreement with the present experimental results.

[1] R. W. P. McWhirter and H. P. Summers, App. At. Coll. Phys., Vol.**2**, 51 (1984).

[2] A.H. Gabriel and C. Jordan, in *Case Studies in Atomic Collisions Physics,* edited by E. W. McDaniel and M. C. R. McDowell, (North Holand Press, 1972), Vol. 2, p. 209.

[3] B. Edlén, Z. Astrophys. **22**, 30 (1942).

[4] K. N. Huang, Y. K. Kim, K. T. Cheng and J. P. Desclaus, Phys. Rev. Lett. **48**, 1245 (1982).

[5] D. P. Das, J. Hata and I. P. Grant, J. Phys. B **17**, L1 (1984).

[6] M. S. Safronova, W. R. Johnson and U. I. Safronova, Phys. Rev. A **54**, 2850 (1996).

[7] M. K. Aly, in *The Solar Corona*, edited by J.W. Evans (Academic Press, New York, 1963).

[8] A. K. Bathia, U. Feldmann and J. F. Seely, At. Data. Nucl. Data Tab. **35**, 453 (1996).

[9] M. S. Safronova, W. R. Johnson and J. F. Safronova, Phys. Rev. A **53** , 4036 (1996).

[10] B. Edlén, Phys. Scr. **28**, 438 (1983).

[11] V. M. Shabaev, Phys. Rep. **356**, 119 (2002).

[12] J. Gillaspy, in *Trapping Highly Charged Ions: Fundamentals and Applications*, (NOVA Science Publishers Inc., 2001).

[13] B. Edlén, Phys. Scr. **26**, 71 (1982).

[14] B. Edlén, Phys. Scr. **28**, 51 (1983).

[15] D. J. Bieber, H. S. Margolis, P. K. Oxley and J. D. Silver, Phys. Scr. **T73** , 64 (1997).

[16] V. Kaufman and J. Sugar, J. Phys. Chem. Ref. Data Vol. **15**, No 1, 321 (1986).

[17] K. T. Cheng, Y. K. Kim and J. Desclaus, At. Data Nucl. Data Tab. **24**, 111 (1979).

[18] K. Butler and C. J. Zeippen, Astrophys. Supp. Ser. **108**, 1 (1994).

[19] J. T. Jefferies, Mem. Soc. R. Sci. Liege **17**, 213 (1969).

[20] G. Wlerick and C. Fehrenbach, in *The Solar Corona*, edited by J.W. Evans (Academic Press, New York, 1963).

[21] G. M. Nikolsky, R. A. Gulyaev and K. I. Nikolskaya, Solar Phys., **21** , 332 (1971).

[22] B. Lyot and A. Dollfus, C. R. Acad. Sci. Paris **237**, 855 (1953).

[23] M. H. Prior, J. Opt. Soc. Am. B **4**, 144 (1987).

[24] C. Z. Dong, S. Fritzsche, B. Fricke and W. D. Sepp, Phys. Scr. **T92,** 294 (2001).

[25] W.R. Johnson and G. Soff, At. Data and Nucl. Data Tables **33,** 405 (1988).
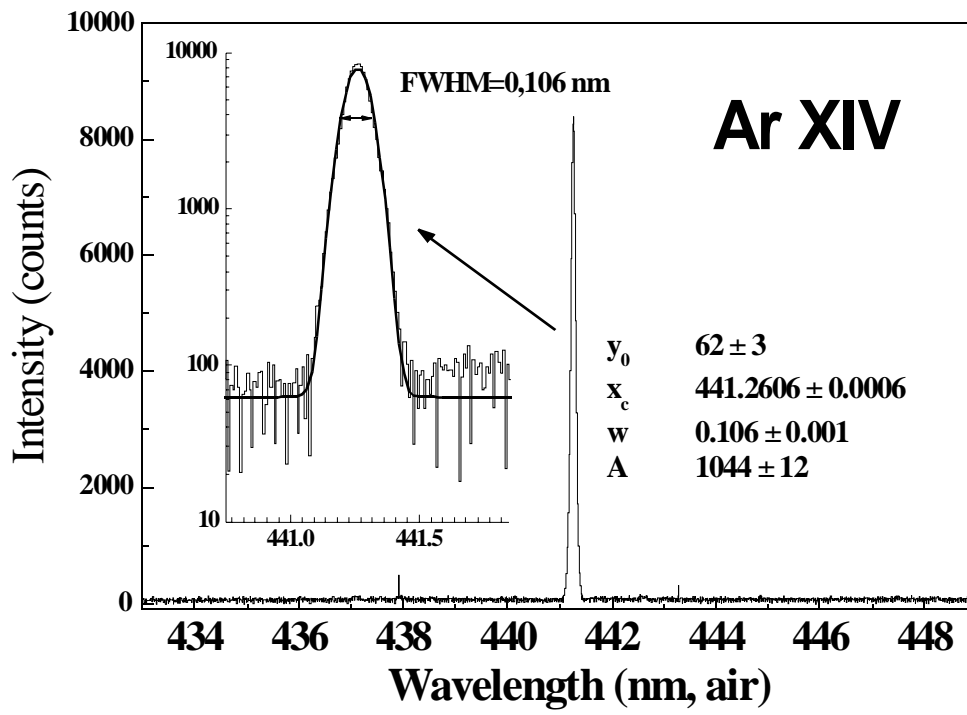
Fig. 1
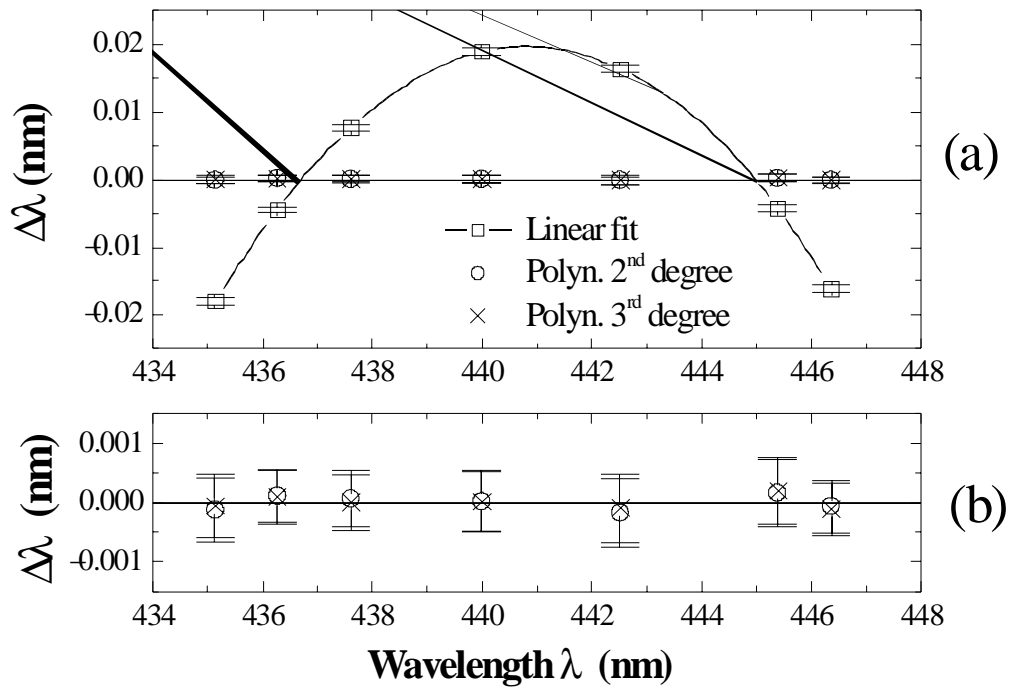
Fig.2

Table 1

Source	Contributions to wavelength uncertainty (10^{-4} nm)			
Ion	Ar^{9+}	Ar^{10+}	Ar^{13+}	Ar^{14+}
Line centroid determination	1.1	0.9	0.6	3.3
Standard deviation of dispersion function	1.1	1.6	0.2	0.9
Calibration wavelength uncertainty	0.4	10	0.1	0.7
Calibration systematic uncertainty	0.3	0.1	0.2	0.5
Total	**2**	**12**	**1**	**5**

Table 2

Ion	Transition	Measured wavelength, (nm, air)		Theoretical wavelength, (nm, air)		
		This work	Others	**This work**	Others	
Ar +9 (F–like)	$2s^2\,2p^5$ $^2P_{3/2} - {}^2P_{1/2}$	**553.3265±0.0002**	553.34±0.02 [19]	**554.75[1],** **554.20[2]** **553.80[3]**	553.339 [16]	
Ar +10 (O–like)	$2s^2\,2p^4$ $^3P_2 - {}^3P_1$	**691.6878±0.0012**	691.686±0.006 [15]	**693.24[1]**	687.3 [17]	
			691.7 [20]	**692.86[2]**	691.8 [18]	
			691.72 [21]	**692.28[3]**	691.6 [14]	
Ar +13 (B–like)	$2s^2\,2p$ $^2P_{1/2} - {}^2P_{3/2}$	**441.2559±0.0001**	441.250±0.003 [15]		438.7 [17]	441.1 [6]
			441.26±0.02 [22]		442.1 [4]	441.65 [24]
		441.2563±0.0004*	441.132±0.2 [23]		441.2 [5]	441.32 [14]
			441.32±0.2 [24]			
Ar +14 (Be–like)	$2s\,2p$ $^3P_1 - {}^3P_2$	**594.3880±0.0005**	594.373±0.004 [15]	**596.46[1]**	594.5 [8]	594.0 [9]
			594.4 [7]	**594.79[2]**	594.37 [10]	597.9 [17]

[1] Calculation using zero order approximation. [2] Calculation including valence–shell correlation. [3] Calculation including core–valence and core–core correlation. * A recent independent measurement.

Table 3

11

Ion	CIDF (cm^{-1})	QED (cm^{-1})	Total	QED (nm)	Theory, (nm, air)	Experiment, (nm, air)
Ar^{+13}	22612.8(12.0)	49.5(7.0)	22662(14)	−0.96	**441.14(27)**	**441.2559(1)**
Ar^{+14}	16770.9(3.0)	53.4(8.0)	16824.3(8.5)	−1.89	**594.22(30)**	**594.3880(3)**

Ar^{+13}	22612.8(12.0)	49.5(7.0)	22662(14)	−0.96	**441.14(27)**	**441.2559(1)**
Ar^{+14}	16770.9(3.0)	53.4(8.0)	16824.3(8.5)	−1.89	**594.22(30)**	**594.3880(3)**

Captions:

Fig.1: An example of a typical line shape (single exposure) for a forbidden transition measured in this work. The insert shows a Gaussian fit in logarithmic scale.

Fig.2: Residuals from the dispersion function fitting, using a linear (solid square) dependence, a second (solid circle), and third degree polynomial (cross). a) all the cases. b) shows only second degree and third degree polynomial fitting residuals in an enlarged scale. Each single exposure includes two such calibration fits.

Table 1: Error budget: main error sources and contributions to the final uncertainties of the wavelengths.

Table 2: Experimental and theoretical results of this work in comparison with other existing data.

Table 3: Results of the configuration interaction Dirac–Fock and QED calculations from this work.